

# Investigation on stability of weld morphology, microstructure of processed zones, and weld quality assessment for hot wire gas tungsten arc welding of electrolytic tough pitch copper

Raghavendra Darji<sup>a,b</sup>, Vishvesh Badheka<sup>a</sup>, Kush Mehta<sup>id a,c</sup>, Jaydeep Joshi<sup>d</sup>, Ashish Yadav<sup>d</sup>, and Arun Kumar Chakraborty<sup>d</sup>

<sup>a</sup>Department of Mechanical Engineering, School of Technology, Pandit Deendayal Energy University (Formerly Known as Pandit Deendayal Petroleum University), Gandhinagar, India; <sup>b</sup>Department of Metallurgical and Materials Engineering, Faculty of Technology and Engineering, The M S University, Baroda, India; <sup>c</sup>Mechanical Engineering, School of Energy Systems, Lappeenranta-Lahti University of Technology (LUT University), Lappeenranta, Finland; <sup>d</sup>ITER-India, Institute of Plasma Research, Ahmedabad, India

## ABSTRACT

In the present investigation, stability of weld morphology was investigated in case of electrolytic tough pitch copper (12 mm thickness) processed by Hot Wire Gas Tungsten Arc Welding (HW GTAW) using CuNi filler wire with variations of processing conditions, using different combination of hot wire's parameters such as feed rate and current. The assessment of weld bead geometry was performed using visual examination (during and after welding), and macrographic dimensional measurements of weld bead geometry such as depth of penetration and depth to width ratio. In addition to the stability of weld bead geometries, microstructural variations and weld quality assessments were studied using optical microscopy, scanning electron microscopy, energy dispersive x-ray spectroscopy, and micro-hardness measurements in case of processed sample observed with most uniform weld bead geometry. The results revealed that minimum dimensional variations of weld bead geometry throughout the processed length was obtained with 5.42 mm bead width, 1.2 mm bead height, 1.8 mm penetration, and 0.36 depth to width ratio when hot wire's parameters were 0.6 m/min wire feed rate and 90 amps hot wire current. The bridging mode of metal transfer helps to receive more stable weld bead geometry with minimum dimensional variations. Ni filler wire of HW GTAW improves the hardness in the Heat affected zone (70 HV<sub>0.3</sub>) and weld zone (80 HV<sub>0.3</sub>), which were 33% and 17% higher of base material. The weld zone was consisting of mixed mode of grains such as dendrites just above the fusion line and cellular grains further above dendrites in case of processed sample of minimum dimensional variations of weld bead geometry throughout the processed length.

## ARTICLE HISTORY

Received 11 December 2020  
Accepted 29 August 2021





## KEYWORDS

Copper; hot; wire; GTAW; weld; bead; shape; Weld; penetration; depth to width ratio; microstructure

## Introduction

Gas Tungsten Arc Welding (GTAW) is a stable and spatter free process due to independent arc ignition by the non-consumable tungsten electrode,<sup>[1]</sup> and because of gas shielding, the process is applied to a wide range of metals and alloys including highly reactive metals.<sup>[2,3]</sup> Despite of the wide range of applicability, the process has to deal with low deposition rate being nonconsumable process. In order to overcome the limitation of low deposition rate, the Hot Wire Gas Tungsten Arc Welding (HW GTAW) was developed.<sup>[4]</sup> In the HW GTAW process, the filler wire is heated to 300–500°C before entering into the weld pool, which leads to improved deposition rate as that of the cold wire GTAW.<sup>[5]</sup> As the filler wire enters preheated into the weld pool, it melts with less amount of heat from the arc (i.e. GTAW power source), which in turn improves the melting rate and increases the deposition rate of filler wire as compared to conventional GTAW.<sup>[1]</sup> In case of HW GTAW, the preheated

filler wire generates the three different modes of metal transfer, namely, free, touching and bridging which in turn influence process stability and weld bead geometry, as reported in the literature of.<sup>[5,6]</sup> In case of free mode of metal transfer, the filler wire forms a small globule at the tip before it enters to welding arc; and subsequently, detaches from the filler wire due to arc force that goes to the weld pool as a single droplet.<sup>[6]</sup> Whereas in touching mode, the similar globule forms at the tip that touches to the surface of the workpiece periodically with continuous wire feeding. In case of bridging mode, the filler wire melts into the weld pool, hence, it provides stability to the weld pool and uniform weld bead geometry.<sup>[5,6]</sup> Additionally, the HW GTAW process is observed as one of the best suitable methods for highly conductive metals and alloys because of preheating of the filler wire.<sup>[6]</sup> Therefore, material like Cu consisting of high thermal conductivity such as 397 W/mK is possible to weld using HW GTAW.<sup>[7]</sup> The need of Cu welding

**CONTACT** Vishvesh Badheka  [drvishvesh@gmail.com](mailto:drvishvesh@gmail.com)  Department of Mechanical Engineering, School of Technology, Pandit Deendayal Energy University (Formerly Known as Pandit Deendayal Petroleum University), Gandhinagar, India; Kush Mehta  [kush.mehta@lut.fi](mailto:kush.mehta@lut.fi)  Mechanical Engineering, School of Energy Systems, Lappeenranta-Lahti University of Technology (LUT University), Lappeenranta, Finland

Abbreviation GTAW: Gas Tungsten Arc Welding; HW GTAW: Hot Wire Gas Tungsten Arc Welding; CMT: Cold Metal Transfer; HAZ: Heat Affected Zone; WZ: Weld Zone; ITER: International Thermonuclear Experimental Reactor; WFR: Wire Feed Rate; HWC: Hot Wire Current; DOP: Depth of Penetration; D/W ratio: Depth/Width ratio; SEM: Scanning Electron Microscopy; EDS: Energy Dispersive x-ray Spectroscopy

© 2021 The Author(s). Published with license by Taylor & Francis Group, LLC.

This is an Open Access article distributed under the terms of the Creative Commons Attribution-NonCommercial-NoDerivatives License (<http://creativecommons.org/licenses/by-nc-nd/4.0/>), which permits non-commercial re-use, distribution, and reproduction in any medium, provided the original work is properly cited, and is not altered, transformed, or built upon in any way.

is justified for engineering applications, because of extraordinary properties such as moderate strength, good corrosion resistance, excellent electrical conductivity, very good appearance, and the absence of ductile to brittle transition behavior which make it the most suited material for the nuclear components.<sup>[8]</sup> The Cu and its alloys are also applied to structural components, electronic components, electrical cables, bus bars, household accessories, and many more upcoming applications are in line too.<sup>[9–13]</sup>

Agreeing to the above specified properties and applications of Cu, welding of Cu through fusion welding is very challenging due to unstable weld pool and high thermal conductivity. In case of laser based welding processes (such as laser arc hybrid welding and laser beam welding), poor weldability issues related to Cu are addressed in.<sup>[14,15]</sup> Some of the major issues related to Cu welding are addressed as follows.

Instability of the weld pool in case of Cu welding causes defects in the weld zone such as pores, spatters and poor weld bead finish due to weld metal ejection.<sup>[14,16]</sup> Wherein, this instability of the weld pool is caused due to inherent properties of Cu such as low viscosity, surface tension<sup>[17]</sup> and dynamic absorptivity.<sup>[18]</sup> Additionally, Cu has very high thermal conductivity (such as 397 W/mK) that in turn leads to high heat dissipation when subjected to welding. Therefore, preheating is recommended in order to decrease the rate of heat dissipation and to have more concentrated heat at welding location. Additionally, high heat input conditions (that is possibly caused by higher current or higher voltage or slower travel speed or combination of all these), which are recommended in case of arc based welding of Cu. Hence, it can be stated that the combination of preheating and high heat input conditions create much more favorable conditions required for adequate heat concentration to successfully weld Cu material.<sup>[19,20]</sup>

On the other side, these conditions of initial preheating and high heat input from process parameters are not advisable from metallurgical point of views, as it adversely affect the metallurgical zones in the vicinity of the weld zone by causing very slow rate of cooling. Furthermore, this slow cooling rate results in coarsening of the grains at the Heat Affected Zone (HAZ) and Weld Zone (WZ) which in turn results into poor mechanical properties. This issue is applicable to any fusion based welding processes, especially reported with laser arc hybrid process, laser beam welding or GTAW.<sup>[7,15,19,20]</sup> In case of GTAW of Cu, another critical issue is cracking in the weld zone as reported by Yinan et al.<sup>[21]</sup> This issue is reported because of the excess amount of oxygen and the prolonged time in the brittle temperature range, cracking occurred during the time of solidification. The formation of cuprous oxide in the weld zone is responsible for cracking as it acts as a eutectic during the solidification of the T3 Cu (99.7 Wt %) weld metal. Nevertheless, this problem of cracking was not observed by Darji et al.,<sup>[15]</sup> wherein the Keyhole GTAW was used as processing technology for 6-mm-thick electrolytic tough pitch Cu. In this study, 100% argon was used as a shielding gas. Argon consisting of higher density acted as a barrier between the liquid weld pool and atmospheric gases.

It can be summarized that GTAW-related variants can be considered as a potential technological solutions for above mentioned challenges, which opens new solutions for

industrial applications with great ease, flexibility, and cost savings as compared to existing technologies. It can be noted that HW GTAW is not investigated for highly conductive materials such as Cu for its stability of weld morphology, microstructure of processed zones and weld quality assessment, hitherto to the best of authors' knowledge. Therefore, it is worth to investigate HW GTAW of Cu analyzing stability of weld morphology, microstructure and weld quality assessment using processing-geometry-properties correlations. The influence of hot wire power source's process parameters is investigated in this study to evaluate the processing capability of HW GTAW on Cu, which is also attempted for the first time to the best of authors' knowledge. The effect of hot wire's process parameters is investigated for variations in weld bead geometry, microstructure and properties. In addition, the effect of Cu-Ni filler wire on the microhardness and microstructure of the weld and HAZ are studied, in the present investigation. These objectives are developed to establish HW GTAW procedure for the Cu components' application of the diagnostic neutral beam of International Thermonuclear Experimental Reactor (ITER).

## Materials and methods

### Base materials, filler wire and accessories

Electrolytic tough pitch Cu was used as base material for the welding experiments in 100 mm X 50 mm X 12 mm size. The chemical composition of the base material is mentioned in Table 1. Cupronickel (70% Cu – 30% Ni) filler wire of 1.2 mm diameter was selected for the HW GTAW. Table 2 presents the chemical composition of the cupronickel filler wire. The tungsten electrode categorized as EWLa – 2, consisting of 4.0 mm diameter and a 25° angle of tip was used in the experimental study. K type thermocouple was used to measure the temperature during the welding, which was fixed as shown in Fig. 1(c). Carbon steel plate kept below the Cu plates as a backing. The shielding gas was ultra-high purity argon gas.

### Experimental setup and methodology

Experimental setup of Fronius make equipment used as HW GTAW, wherein a main power source of Fronius TT5000, and power source for filler wire of Fronius TT2200 with filler wire feeder of KD 4000D-11 were used. Figure 1(a) shows overall experimental setup with power sources, wire feeder system, shielding gas system, torch, oscillating system, and table for workpiece. Figure 1(b) shows Close view of photograph

**Table 1.** Chemical Composition of the ETP copper.

Element	Copper	Lead	Phosphorous	Silicon
Amount in (Wt %)	99.988	0.001	0.004	0.003

**Table 2.** Filler wire chemical composition.

Elements	Manganese	Silicon	Nickel	Copper	Iron	Phosphorous
Percentage (Wt %)	0.806%	0.128%	29.890%	68.660%	0.400%	0.01%

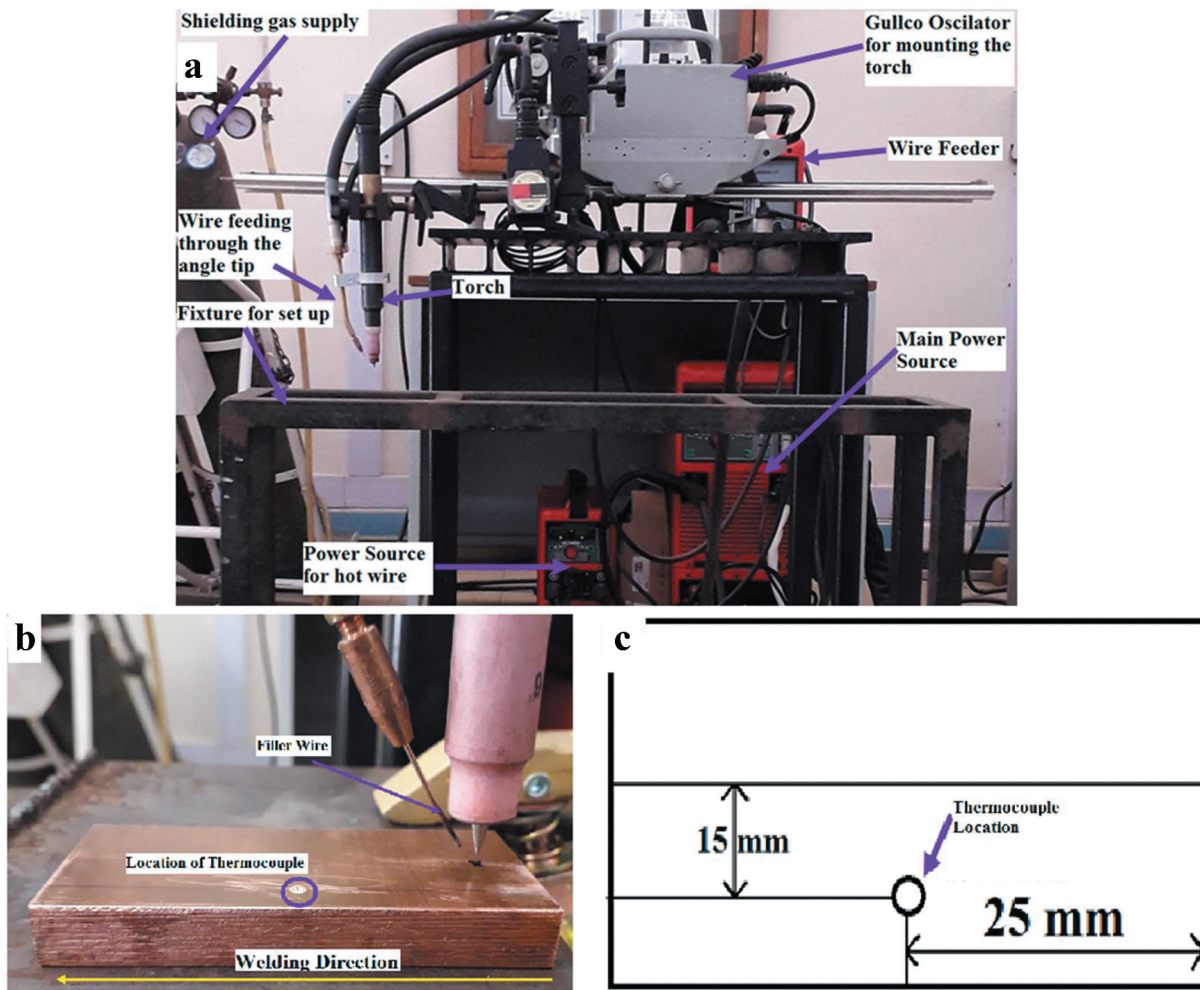


**Figure 1.** Experimental details. (a) Experimental setup, (b) close view of photograph showing base material, electrode-filler wire setup, (c) location of thermocouple for temperature measurements during the experiments.

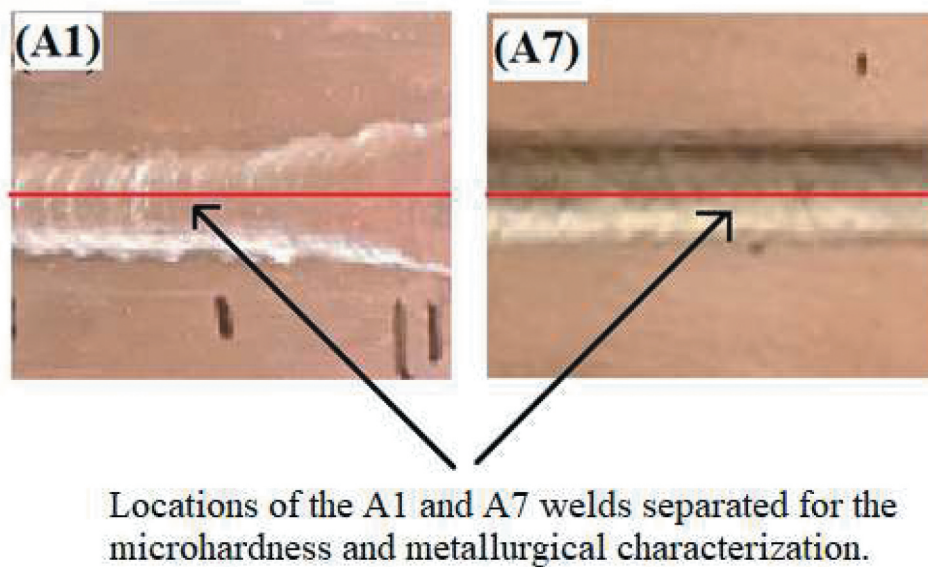


**Figure 2.** Surface appearance of A1 and A7 welds showing difference in weld bead surface geometry.

showing base material, electrode-filler wire setup. As a standard procedure, the tungsten electrode and the filler wire were connected to the negative terminals of their

respective power sources. Figure 1(c) shows the dimensions indicating location of the K type thermocouple mounted for measuring the temperature during experiments.

**Table 3.** Process parameters of GTAW power source.

Sr. No	Parameter	Values
1	Welding current (Amp)	300
2	Tungsten to base plate distance (mm)	1–2
3	Voltage (V)	14.4–16.3
4	Welding speed (mm/min.)	120
5	Preheat condition ( $^{\circ}$ C)	175
6	Filler wire stick out (mm)	10
7	Tungsten electrode stick out (mm)	25
8	Filler wire feeding angle ( $^{\circ}$ )	30

**Table 4.** Experimental conditions with different variations of process parameters.

Parameter/sample Id	A1	A2	A3	A4	A5	A6	A7
Wire feed rate (m/min.)	No	0.4	0.4	0.4	0.6	0.6	0.6
Filler wire current (Amp)	Filler used	30	60	90	30	60	90
	Filler used						

**Table 5.** Filler wire voltage recorded through data monitoring system connected to power source of hot wire in HW GTAW setup.

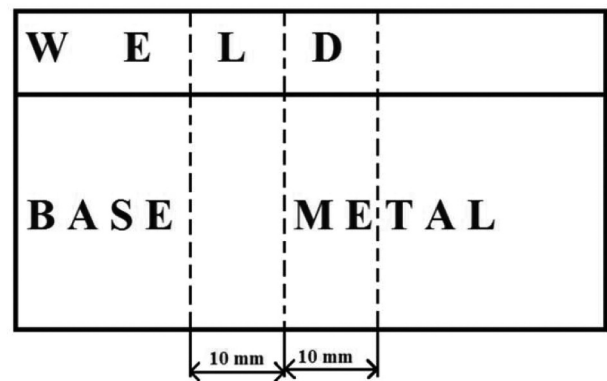
Experiment	A1	A2	A3	A4	A5	A6	A7
Filler wire voltage (V)	Not applicable	1.7t–2.1	1.3t–1.8	5.2t–6.4	2t–2.8	1.2t–2.0	1.2t–1.5

There were seven different combinations of parameters planned for the experiments, wherein one autogenous welding with GTAW and six HW GTAW experimental conditions with the varying hot wire conditions were selected (Fig.2). The process parameters for GTAW power source were kept constant as presented in Table 3. The experimental conditions are varied using Wire Feed Rate (WFR) and Hot Wire Current (HWC) of hot wire power source, as presented in Table 4. The selected values were 0.4 m/min and 0.6 m/min in case of WFR, and HWC were 30 amps, 60 amps, and 90 amp.

The preheating was applied using GTAW torch at the start position of the weld, as mentioned in previous study of Darji et al.<sup>[15]</sup> The preheating temperature of 175 $^{\circ}$ C was obtained when GTAW torch was applied to the start position for 20 seconds with welding current of 300 amp. Therefore, delay time in filler wire feeding was kept as 20 seconds. The preheating temperature of 175 $^{\circ}$ C was identified as suitable preheating temperature based on initial experimental observation, where adequate melting of material to form weld pool was observed. This preheating temperature was kept constant during experimentation for aforementioned seven conditions. During the experiments, filler wire voltage variations were monitored from respective power source and noted in the Table 5.

### Post weld testing and characterization

All the welds were examined visually after the experiments for the surface defects such as appearance of weld beads, surface porosities, and irregular width and height. After the visual examination, weld surface features with measurements on weld bead width and weld height were measured without cutting the samples. Measurements for the weld surface features were carried out at every 10 mm distance on the weld processed surface throughout the length of the weld (excluding 15 mm from start and end) using Dial Calliper. Total seven measurements

**Figure 3.** Locations of the microhardness measurement.

per weld bead were carried out, and an average value was presented for each weld bead. After the measurements on weld surface features, the cross sections of all the welds were analyzed, wherein the extraction of each weld was conducted from the center of the weld length and from the transverse to the welding direction. These extracted specimens were processed with mechanical grinding (rough grinding followed by fine grinding, polishing, and etching), wherein the polishing was performed using alumina slurry and etching was performed by potassium dichromate as a part of metallography procedure to examine macro-micro structures and observations with measurements. On the prepared cross sections, the Depth of Penetrations (DOPs) and Depth to Width ratios (D/W ratios) were measured.

The weld samples observed with narrow bead width, deep penetration, and higher D/W ratio were, carried forward for the macro examination, microhardness measurements and microstructural study. Macrostructure examination was conducted using a stereomicroscope (Benbros Engineering, BSA A model). Microhardness was measured at three different locations across the weld cross section (see Fig. 3, three locations 10 mm apart), by applying 300 grams load at 0.5 mm interval, for 10 seconds (ESEWAY make, Model Nexus 4302, Vickers hardness testing), and the average values of three measurements were presented. Afterward, the optical microscopy (using Olympus make, model G51) was performed on welds with different magnifications (such as 100 $\times$  and 500 $\times$ ). The Scanning Electron Microscopy (SEM) was also performed to study the solidification mode and subsequent Energy Dispersive x-ray Spectroscopy (EDS) was performed for elemental mapping in the weld, HAZ and base metal to study the effect of Ni addition (using JEOL SEM model no. JSM7600F).

## Results and discussion

### Visual appearance

Figure 4 presents the visual appearance of welded samples that are attained for all the experimental conditions. It can be seen that A1 was observed with surface voids at the beginning which was performed in an autogenous mode. These surface voids can be identified as porosities, which were may be due to the turbulence generated by the Cu molten pool having low viscosity.<sup>[17]</sup> This turbulence within the weld pool increases chances of interaction with oxygen from atmosphere, which in turn results into porosity. In the beginning of welding, the

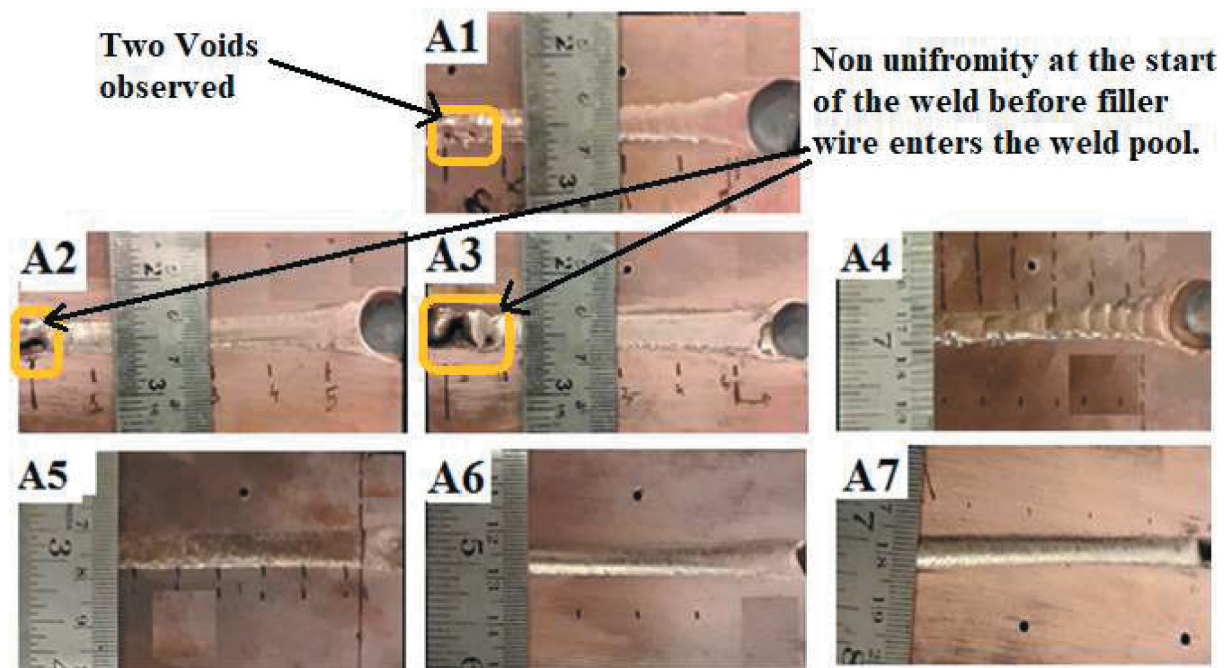


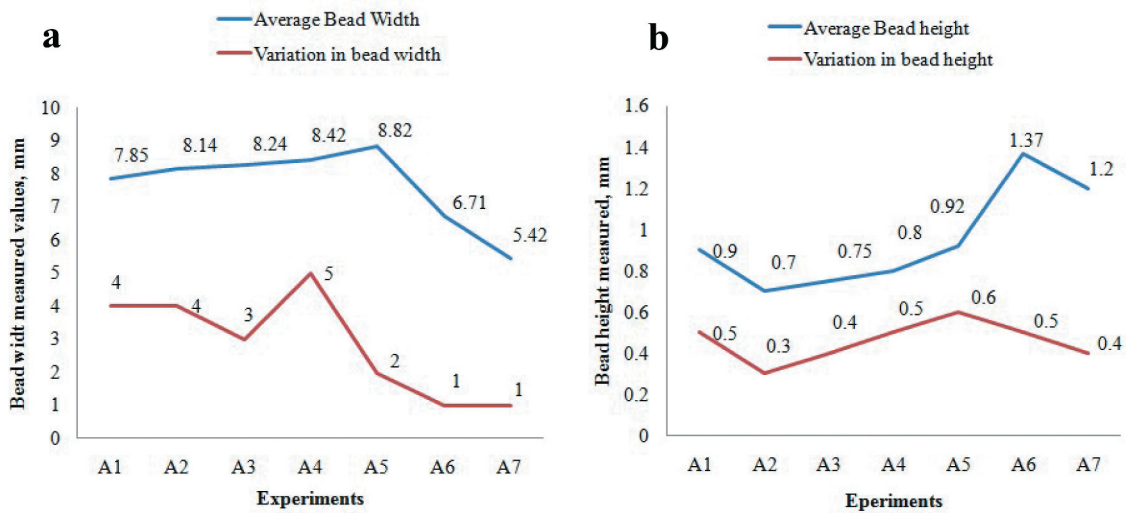
Figure 4. Surface appearance of weld bead profiles for seven different conditions of A1–A7. (identification numbers are as per Table 4).

process is unstable and that may be the reason for porosities at the beginning of the weld in case of A1. Apart from the A1, in case of A2–A7, the valley type feature was observed as instability of weld at the start of every weld, which was formed during the preheating stage that can be avoided using run on tabs. On the other side, rest of the weld length was observed as defect free without any evidence of surface defects. These defect free weld beads can endorse the stability of the HW GTAW process. As a reflection on weld bead profile, it can also be stated that the weld pool behavior was maintained the stability when preheated filler wire was added (i.e. in case of A2–A7 results as compared to A1). Also, the limitation of GTAW such as wide and shallow weld bead was improved with narrow and deeper penetration by adding hot wire filler wire and controlling the flow of the molten Cu inside the weld pool. The similar controlled flow of the molten metal was resulted with more stable weld bead geometry as observed in K-GTAW (without application of filler wire).<sup>[15]</sup> During the experiments, it was observed that there were no other effects such as arc blow or bypass arc, which generally observed in case of multiple power source welding (for instance, Wang et al.<sup>[5]</sup>). Therefore, the arc was stable during HW GTAW and resulted into controlled weld bead geometry. Minor variations in weld bead profiles were observed as can be seen from Fig. 4, which were may be due to secondary power source parameters of hot wire working with primary power source.

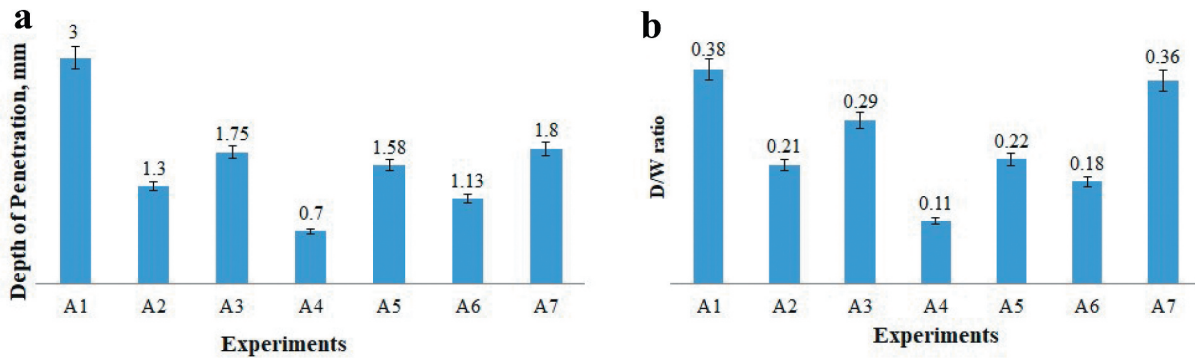
#### Dimensional measurements of DOP and D/W ratio

Figure 5(a,b) show the average measured value and variation along the lengths in measured value for the weld bead width and height in case of A1–A7 conditions. A1 was observed with weld bead width of 7.85 mm average value and 4 mm variation in width, and 0.9 mm weld bead height and 0.5 mm variation in height. In case of hot wire conditions of A2, A3, and A4,

average weld bead widths were observed as 8.14 mm, 8.24 mm and 8.42 mm with 4 mm, 3 mm and 5 mm variations respectively, and average weld bead heights were 0.70 mm, 0.75 mm and 0.80 mm with 0.30 mm, 0.40 mm, and 0.50 mm variations, respectively. In case of other hot wire conditions of A5, A6, and A7, the average weld bead widths were observed as 8.82 mm, 6.71 mm and 5.42 mm with 2 mm, 1 mm, and 1 mm variations, respectively, and average weld bead heights were 0.92 mm, 1.37 mm and 1.20 mm with variations of 0.60 mm, 0.50 mm, and 0.40 mm, respectively. These results show that, the weld condition of low WFR (0.4 m/min) was resulted with the wider and shorter weld beads, whereas the weld condition of high WFR (0.6 m/min) was resulted with the narrow and larger weld beads. The deviation in the bead widths and heights were observed small in case of 0.6 m/min WFR, which suggest that the weld bead shape obtained through 0.6 m/min WFR was more stable as compared to 0.4 m/min WFR. In case of A2, A3, and A4, the volume of the filler wire entered into the weld pool was less. Consequently, it consumes less amount of heat from the arc to get melted, wherein major amount of heat was transferred to the base metal of Cu that in turn resulted in formation of a large size weld pool throughout the length. The similar phenomena of wider weld pool throughout the length (i.e. with the progression of the welding) was also reported by Darji et al.<sup>[15]</sup> during the keyhole GTAW of Cu. While in case of A5, A6 and A7, the weld bead was observed with less variations with respect to widths and heights. As the WFR of 0.6 m/min was higher as compared to WFR of 0.4 m/min, the filler wire entered into the weld pool was higher. Therefore, as smaller amount of filler wire was participated into the weld pool in case of conditions A2, A3 and A4 (that were performed with 0.4 m/min WFR) as compared to A5, A6, and A7 conditions (that were performed with 0.6 m/min WFR). Proportionately more heat from the welding arc utilized for melting of the filler wire that created the conditions where the



**Figure 5.** Graphs indicating measurements of weld bead dimensions for different experimental conditions (A1–A7s) mentioned in Table 4, (a) bead width measurements, (b) bead height measurements.



**Figure 6.** Graphs indicating DOP and D/W ratio measurements (a) DOP observed for different experimental conditions A1–A7 mentioned in Table 4, (b) D/W ratio for different experimental conditions A1–A7 mentioned in Table 4.

less heat transferred to the base metal, consequently slender weld pools have formed and filler wire added to it. Thus, on the basis of the bead dimension measurements, it can be recognized that the 0.6 m/min WFR resulted to more uniform weld bead geometry as compared to other investigated conditions.

DOP and D/W ratio were also the crucial parameters which outright the uniformity of the bead geometry. Figure 6 shows the DOP and D/W ratio for investigated experimental conditions. It can be seen that maximum DOP of 3.00 mm and a D/W ratio of 0.38 were observed in case of A1 condition. Among the hot wire conditions, for A2, A3, and A4, the DOP was observed as 1.3 mm, 1.75 mm, and 0.7 mm, respectively, while D/W ratio was observed as 0.21, 0.29, and 0.11 respectively. In case of A5, A6, and A7, DOP was observed as 1.58 mm, 1.13 mm, and 1.80 mm, respectively, and D/W ratio was observed as 0.22, 0.18, and 0.36, respectively. It was noted that, in the case of the DOP and D/W ratio, A3 (0.4 m/min WFR, and 60 amp HWC) and A7 (0.6 m/min WFR, and 90 amp HWC) observed with better results of DOP and D/W ratio. This was because of the mode of metal transfer influenced by the filler wire's parameters to the weld pool.<sup>[5]</sup> There are three metal transfer modes such as free, touching and bridging modes in the HW GTAW,<sup>[6]</sup> which were influenced by filler wire's parameters such as WFR, and HWC.

It was also reflected through variation in filler wire voltage (as that defines the distance between the tip of the filler wire and the surface of workpiece), which was displayed on the Fronius TT2200. The voltage variations were depended on the DOP and the D/W ratio.<sup>[5]</sup> Table 5 shows filler wire voltage observed during the experiments. It can be correlated that the variation in filler wire voltage were depended on mode of metal transfer and that subsequently influenced DOP and D/W ratio. It was interpreted that the lower value of filler wire voltage was observed as a result of smaller gap between filler wire and weld pool, whereas higher value of filler wire voltage was observed as a result of larger gap between filler wire and weld pool, based on literature of.<sup>[5]</sup> In the present study, it was perceived that when the filler wire voltage values were low, the weld bead with improved DOP and D/W ratio were received, such as in case of A3 and A7 conditions. In these conditions of A3 and A7, the variation in the filler wire voltage were small as 1.3 V–1.8 V and 1.2 V–1.5 V, respectively. Whereas, in case of A2, A5, and A6 conditions, the variations of filler wire voltage were large as 1.7 V–2.1 V, 2.0 V–2.8 V, and 1.2 V–2.0 V, respectively. The small variations in filler wire voltage were observed may be because the filler wire was melted after entering into the weld pool through bridging mode of metal transfer.<sup>[5]</sup> In touching mode, the filler wire forms

a globule at the tip of filler wire that goes into the weld pool periodically, and consequently results into low DOP and D/W ratio.<sup>[6]</sup> The metal transfer of free mode was responsible for into poor weld bead geometry that may be the reason for A4 condition, wherein poor weld bead geometry was observed. Also, the received weld bead shape was nonuniform as can be seen from Figs. 4 and Figs 5. The experimental condition for the A4 experiment was 0.4 m/min WFR, and 90 amps HWC (i.e. low WFR, and high HWC), which was responsible for free mode of metal transfer<sup>[5]</sup> that subsequently resulted to poor weld bead geometry. Thus, it can be stated that the WFR and HWC significantly contributed to variations in weld bead geometry.

### Macrostructure examination

Macrostructure examinations of A1 and A7 are shown in the Fig. 7. It can be seen that A1 was resulted with porosities. Miyagi and Zhang,<sup>[22]</sup> Wang et al.<sup>[16]</sup> and Camurri et al.<sup>[23]</sup> had also reported the similar problems of porosities, and voids during the fusion welding of Cu. The porosities were formed may be due to the partial penetration caused by improper arc in case of A1, wherein gases may get entrapped into the weld

pool. Another reason for porosity may be the combined effect from rate of solidification, turbulent weld pool and interaction of weld pool with atmospheric gases. The turbulent weld pool of Cu was occurred in A1 condition that may have interacted with the atmospheric gases, and its quick solidification may have resulted to gases entrapment in the weld pool.

There was no defects observed in the macrostructure of A7, which was produced using the filler wire. It was recommended that the use of compatible filler can stabilize the weld pool and that may be the strong reason to eliminate the possibility of any defects within weld region.<sup>[24]</sup> In case of A7 weld, the use of compatible filler wire was resulted A7 weld as defect free zone. It was may be because of viscous behavior of CuNi filler wire that may have resulted in better and stable material flow within the weld pool during processing and subsequently resulted in defect free weld bead geometry.<sup>[25]</sup> This is also in-line of improved viscous behavior in weld pool that is observed with of Ni and Cu interactions.<sup>[25,26]</sup> The viscosity of the liquid weld pool consist of 70–30 Cupronickel filler wire and Cu base material have generated the stable weld pool, which did not deviate its shape even under the arc force and hence the same is resulted in defect free weld geometry.

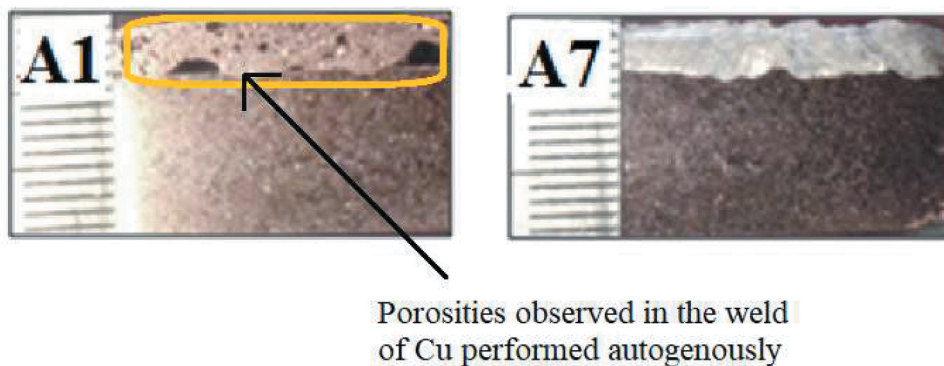


Figure 7. Macrostructure images along the length for A1 and A7.

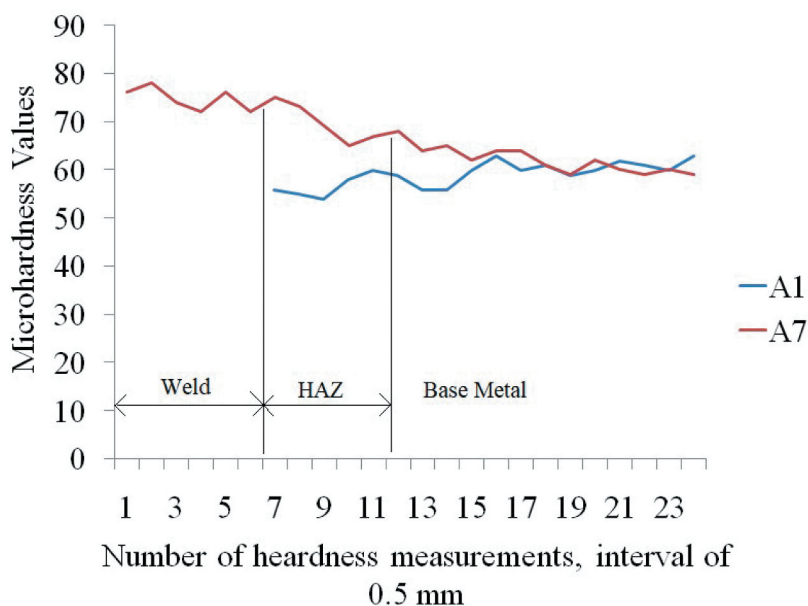


Figure 8. Hardness profile across the welding, HAZ and base material for A1, and A7 conditions.

### Microhardness

Figure 8 exhibits the hardness profiles of A1 and A7 welds. It can be seen that A7 weld attained improved hardness as compared to A1 (comparing HAZ of the two welds, A1 and A7, micro hardness not measured at the weld of A1 due to the presence of porosities). Hardness at the HAZ of A1 ( $55 \text{ HV}_{0.3}$ – $60 \text{ HV}_{0.3}$ ) was very common and it was firmly reported in the

previous studies on Cu welding by fusion welding processes.<sup>[20,27]</sup> This result of the hardness was an outcome of the grain coarsening.<sup>[15]</sup> Contrary to the previous study,<sup>[26]</sup> appealing results were noticed in the weld and HAZ of the A7. The weld hardness was enhanced to 33% ( $80 \text{ HV}_{0.3}$ ) and HAZ hardness improved by 17% ( $70 \text{ HV}_{0.3}$ ) that of the base metal ( $60 \text{ HV}_{0.3}$ ) and the base metal resulted as a softer region.

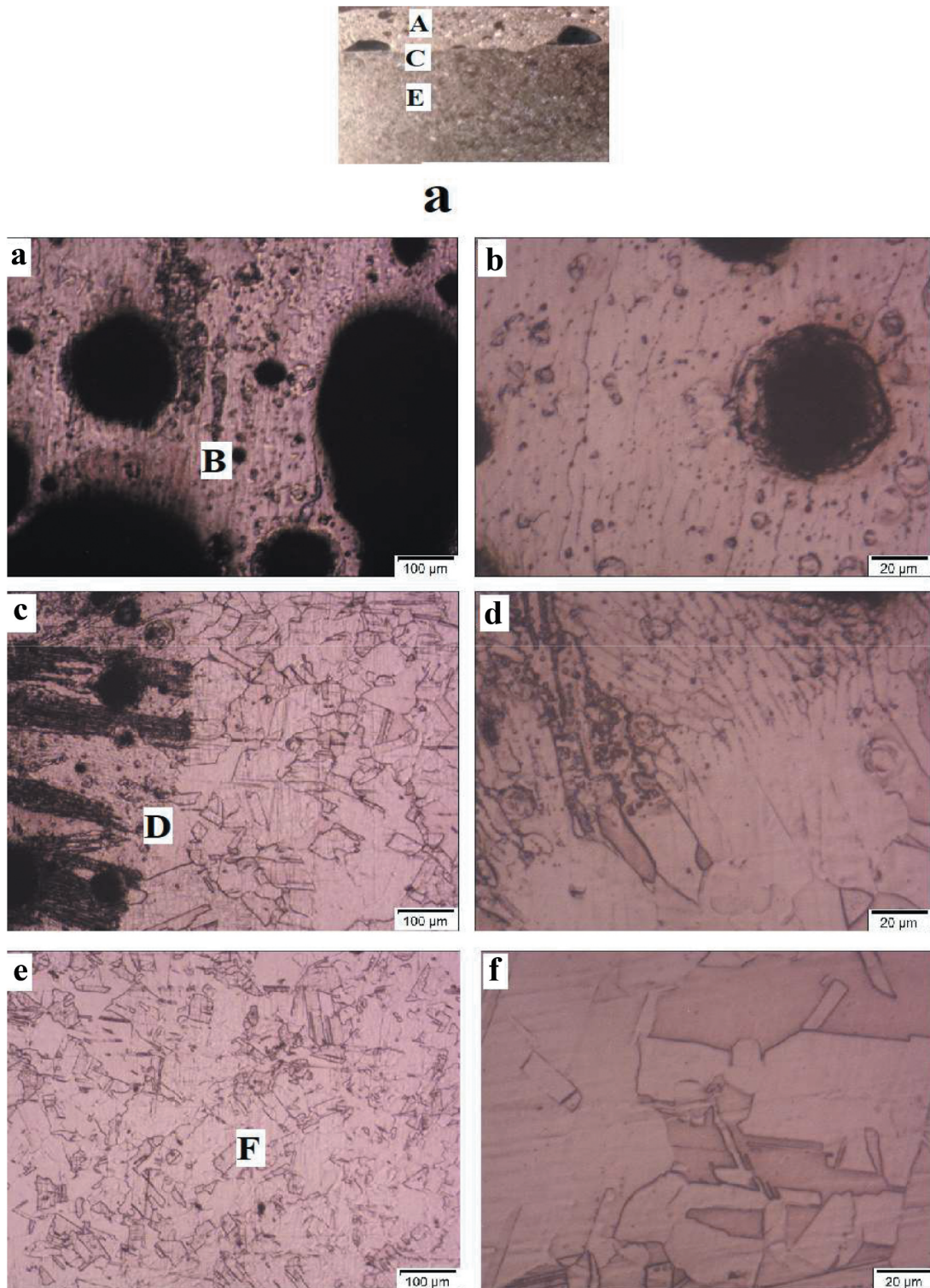
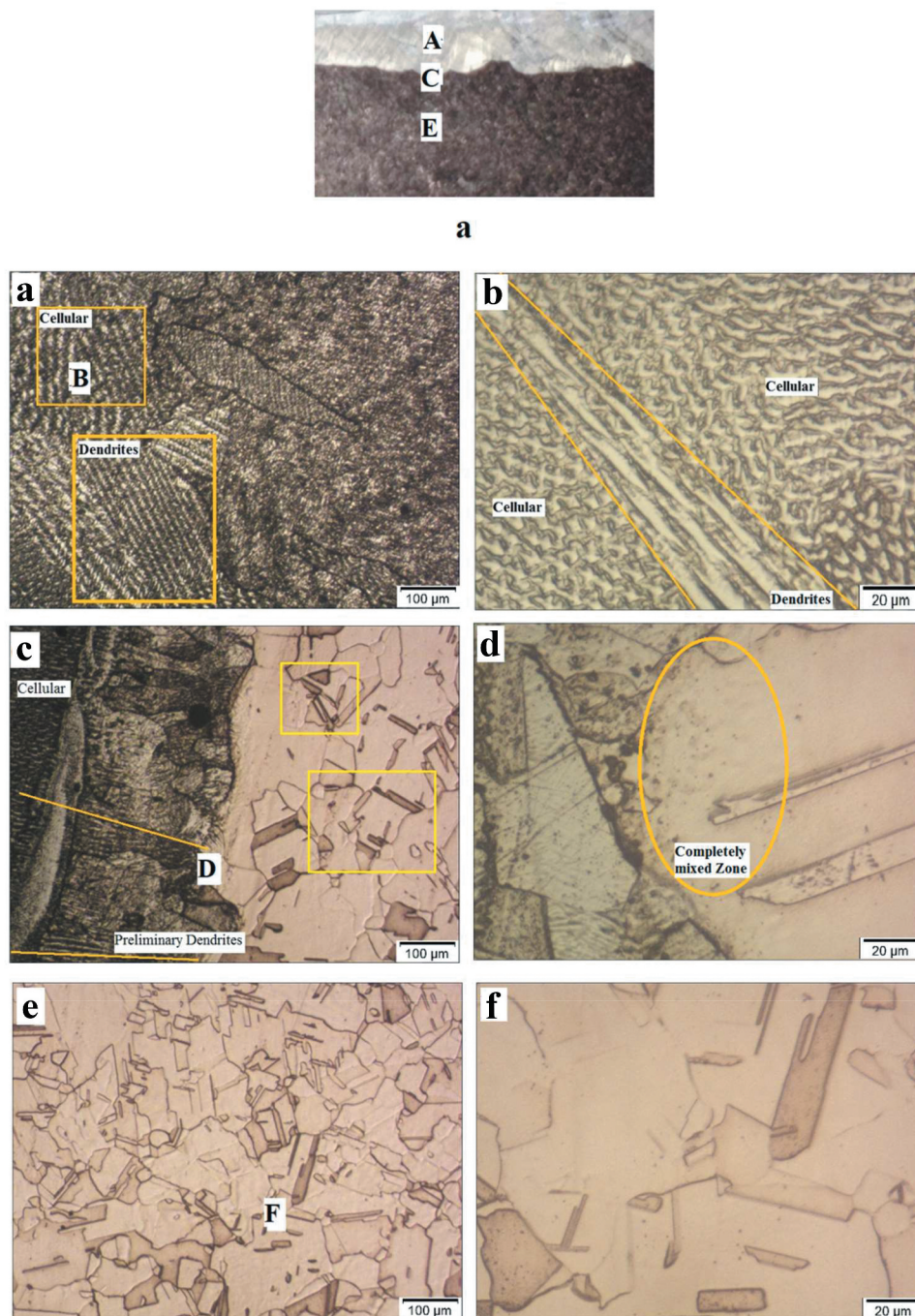


Figure 9. Microstructures images of the A1 weld, (a,b) weld zone, (c,d) HAZ and (e,f) base metal, locations for microstructure are indicated in the macrograph image of a.





**Figure 10.** Microstructure images of the A7 weld, (a,b) weld zone, (c,d) HAZ and (e,f) base metal, locations for microstructure are indicated mapped in the macrograph of a.

This was due to the Ni addition, through filler wire, the addition of Ni had considerably positive effects in the weld and HAZ of A7.<sup>[28,29]</sup> The Ni diffused into the HAZ region of the weld during the cooling of the specimen to the room temperature, as a result HAZ strengthen despite of coarse grains, the Ni generated the frictional resistance for the movement of the dislocation, which in turn strengthen the HAZ.<sup>[29]</sup> This phenomenon was found in A7 weld which discussed in the subsequent sections. The solid solution region of Cu and Ni was also identified by Zhang et al.<sup>[30]</sup> during the diffusion welding of Mo to Cu using Ni interlayer toward the Cu zone.

### Microstructural examination

Figure 9 presents the microstructure images of the A1 weld (locations of the microstructures are shown in the macro section a). The weld region (A and B) of the A1 was observed with porosities. It can be seen that the grain coarsening was observed in the HAZ region (Fig. 9(c,d)), as compared to the base metal (Fig. 9(e,f)). This issue of grain coarsening was the commonly observed as a consequence of the slow cooling rate due to preheating and high heat input.<sup>[7,20]</sup>

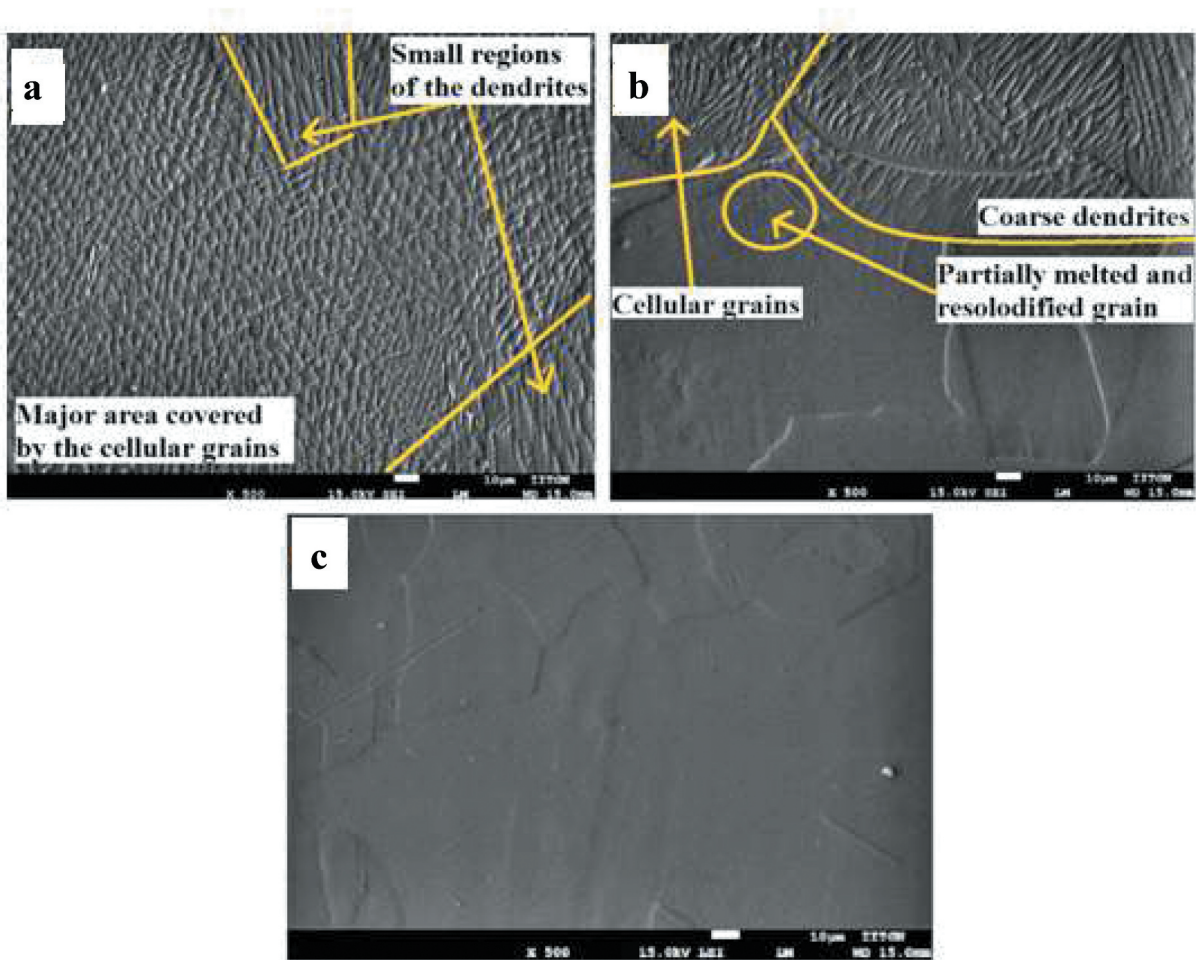


**Figure 11.** SEM images of the A7 condition, (a) weld zone, (b) HAZ, and (c) base metal.

Figure 10 shows the microstructure images of the A7 (macro section **a** shows the locations for microstructure images). It can be seen that the microstructure in the weld is consisting of mixed mode of grain structures Fig. 10(a,b). Columnar dendrites were observed majorly in the weld zone, whereas the cellular grains were also presented. At the fusion line, dendrites were presented due to the epitaxial solidification<sup>[31]</sup> but away from the fusion line, the amount of dendrites was reduced and most of the grains were cellular. This mixed mode of grain structure was resulted because of the high heat input condition by high HWC (90 amps) and initial preheating of 175°C. As a result of high heat input, the dendritic grain growth was reduced as a consequence of temperature gradient.<sup>[32–34]</sup> The grains in the HAZ (C and D) were coarse as well as equiaxed. The weld zone consist of the complete mixed grain structures, which can be considered as a solid solution region. This region was formed because of the mutual solubility between Cu and Ni<sup>[28]</sup> that in-turn may have caused similar crystal structure of Cu and Ni (Face Centered Cubic). Being complete soluble elements, Cu and Ni have formed a solid solution in the weld zone during the welding and in the HAZ through diffusion during the cooling. Microstructure of the base metal (E and F) was obvious consisting of the equiaxed grains having twins.

### Scanning electron microscopy and energy dispersive x-ray spectroscopy

SEM images of the A7 weld shown in Fig. 11. The results obtained from SEM images were in favor of the optical microscopy. Mixed mode of grains was found in which the dendrites were observed just at the fusion line and away from the fusion line with cellular grains. EDS for locations mentioned in Fig. 12(a) is shown in Fig. 12(b). The result shows that the amount of Ni was reduced in the weld zone as compared to the chemical composition of filler wire (as presented in Table 2. During the welding, elements of Ni and Cu were mixed completely in the weld zone.

Apart from the positive results obtained with the Ni addition, the amount of oxygen was also quite low. In the previous study, the amount of oxygen was reported as one of the major factors that may have caused the cracking in the study of.<sup>[21]</sup> In the present investigation, the argon shielding was effective which may have eliminated the gas metal interaction. Furthermore, the filler wire may have stabilized the weld pool, that in turn have resulted with low oxygen content in A7 condition.

### Cooling rate of A7 weld

Figure 13 shows the cooling rate of the A7 condition as 1.17°C/sec. This cooling rate was very slow as compared to the previous study of,<sup>[15]</sup> in which it was 3.31°C/sec. This difference in

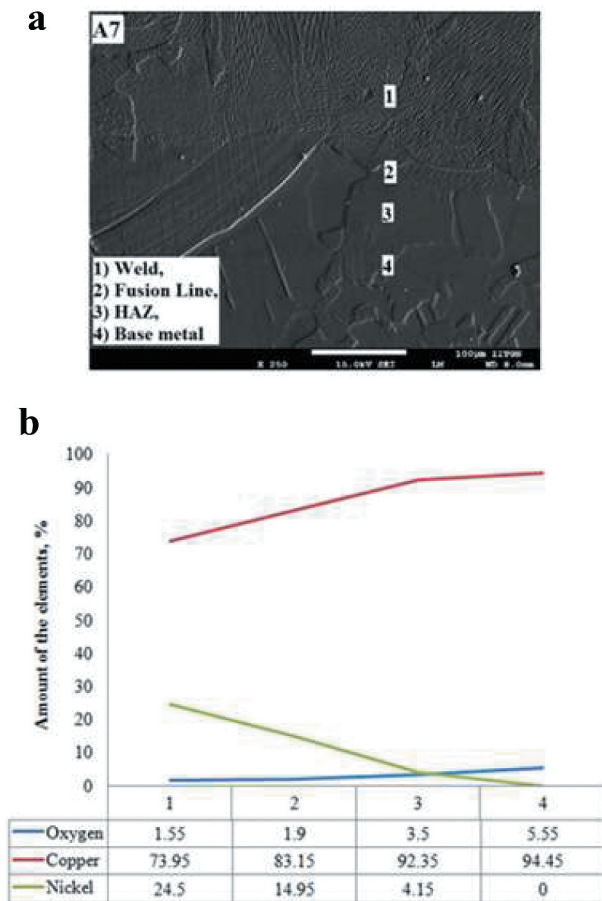


**Figure 12.** (a) SEM image and indicated spots for EDS and (b) EDS results (weight % elements of Cu, Ni, and O<sub>2</sub>) in case of A7 condition.

the cooling rate because of differences in specimen size and welding parameters.<sup>[15]</sup> The slow cooling rate of 1.17°C/ sec may have allowed enough time for the Ni atoms to diffuse into the Cu, which resulted in the solid solution strengthening. Solid solution zone have resulted to improved microhardness in the HAZ wherein Ni was diffused.

## Conclusions

In the present study, investigation on stability of weld morphology, microstructure of processed zones, and weld quality assessment is addressed using hot wire gas tungsten arc welding in case of electrolytic tough pitch copper. Following conclusions can be drawn from this study:

- (1) The minimum dimensional variations of weld bead geometry throughout the processed length were obtained with the 0.6 m/min WFR, and 90 amps HWC, which was having 5.42 mm bead width, 1.2 mm bead height, 1.8 mm DOP, and a 0.36 D/W ratio.
- (2) The weld morphology obtained in case of 0.6 m/min WFR (A5, A6, and A7) was found suitable as less dimensional variations in weld bead width and weld bead height were observed.
- (3) The hardness at HAZ was improved to 17% when Ni filler wire was added, despite the presence of coarse grains in the HAZ. In the weld 33% enhancement in the hardness reported.
- (4) The weld zone was consisting of mixed mode of grains such as dendrites just above the fusion line and cellular grains further above those dendrites in the case of

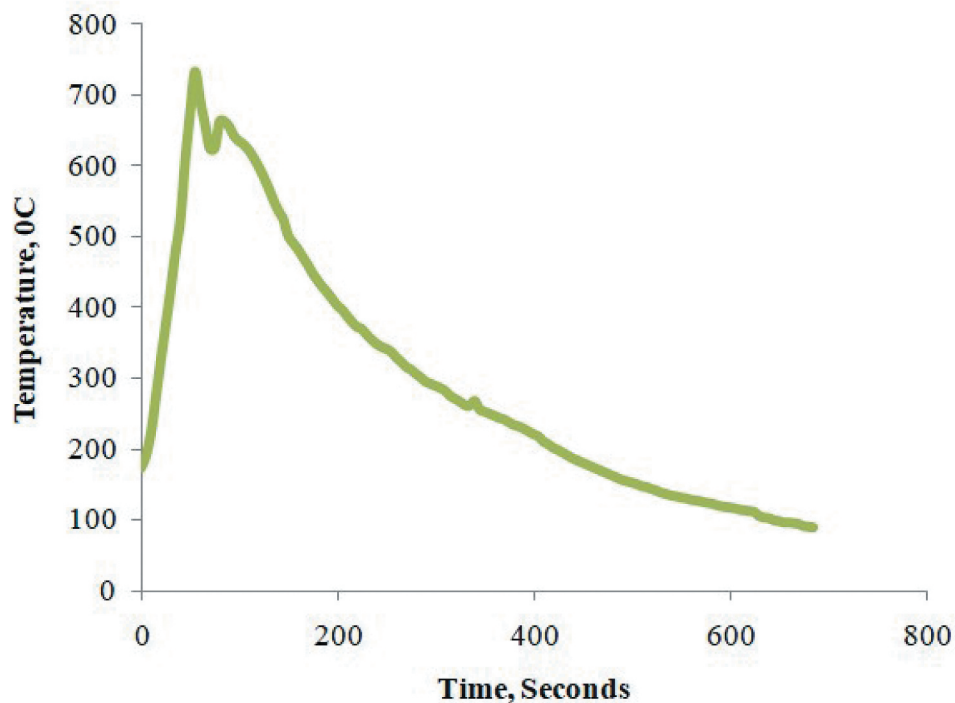


**Figure 13.** Temperature vs time curve during processing in case of A7 condition.

processed sample of minimum dimensional variations of weld bead geometry throughout the processed length. Cellular grains were dominant as compared to the dendrites within the weld zone.

- (5) During the solidification of the weld metal in case of processed sample of minimum dimensional variations of weld bead geometry throughout the processed length, the Ni atoms were diffused in the HAZ due to enhanced solubility of Ni into Cu.

## Acknowledgments

The authors are thankful to the Board of Research in Nuclear Sciences (BRNS), India for funding through project no. 39/14/04/2018-BRNS. Authors are also thankful to the Pandit Deendayal Energy University, Raisan, Gandhinagar, India for the infrastructure and facilities to the affiliated authors.

## Disclosure statement

No potential conflict of interest was reported by the author(s).

## Funding

This work was supported by the Board of Research in Nuclear Sciences [39/14/04/2018-BRNS-39004]. Open access funding is given by LUT University, Finland.

## ORCID

Kush Mehta  <http://orcid.org/0000-0001-6158-8627>

## References

- Spaniol, E.; Ungethüm, T.; Trautmann, M.; Andrusch, K.; Hertel, M.; Füssel, U. Development of a Novel TIG Hot-Wire Process for Wire and Arc Additive Manufacturing. *Weld. World*. 2020, 64(8), 1329–1340. DOI: 10.1007/s40194-020-00871-w.
- Baufeld, B.; Van Der Biest, O. Mechanical Properties of Ti-6Al-4V Specimens Produced by Shaped Metal Deposition. *Sci. Technol. Adv. Mater.* 2009, 10(1). DOI: 10.1088/1468-6996/10/1/015008.
- Bai, J. Y.; Fan, C. L.; Lin, S.; Yang, C. L.; Dong, B. L. Effects of Thermal Cycles on Microstructure Evolution of 2219-Al during GTA-Additive Manufacturing. *Int. J. Adv. Manuf. Technol.* 2016, 87(9–12), 2615–2623. DOI: 10.1007/s00170-016-8633-1.
- Shinozaki, K.; Yamamoto, M.; Mitsuhata, K.; Nagashima, T.; Kanazawa, T.; Bead Formation, A. H. Wire Temperature Distribution during Ultra-High-Speed GTA Welding Using Pulse-Heated Hot-Wire. *Weld. World*. 2011, 55(3–4), 12–18. DOI: 10.1007/BF03321281.
- Wang, H.; Hu, S.; Wang, Z.; Xu, Q. Arc Characteristics and Metal Transfer Modes in Arcing-Wire Gas Tungsten Arc Welding. *Int. J. Adv. Manuf. Technol.* 2016, 86(1), 925–933 DOI: 10.1007/s00170-015-8228-2.
- Lu, Y.; Chen, S.; Shi, Y.; Li, X.; Chen, J.; Kvidahl, L.; Ming, Y. Double-Electrode Arc Welding Process : Principle, Variants, Control and Developments. *J. Manuf. Process.* 2014, 16, 93–108. doi:10.1016/j.jmapro.2013.08.003.
- Auwal, S. T.; Ramesh, S.; Yusof, F.; Manladan, S. M. A Review on Laser Beam Welding of Copper Alloys. *Int. J. Adv. Manuf. Technol.* 2018. DOI: 10.1007/s00170-017-1566-5.
- Butterworth, G. J.; Forty, C. B. A Review Article A Survey of the Properties Reactor Materials of Copper Alloys for Use as Fusion. *J. Nuc. Mat.* 1992, 189, 237–276.
- Joshi, G. R.; Badheka, V. J. Processing of Bimetallic Steel-Copper Joint by Laser Beam Welding. *Mater. Manuf. Process.* 2019, 34(11), 1232–1242. DOI: 10.1080/10426914.2019.1628262.
- Mehta, K. P.; Badheka, V. J. Materials and Manufacturing Processes A Review on Dissimilar Friction Stir Welding of Copper to Aluminum : Process, Properties and Variants. *Mater. Manuf. Process.* 2016, 31 (3), 233–254. doi:10.1080/10426914.2015.1025971.
- Tang, D.; Li, J.; Wang, L.; Wang, Z.; Kong, C.; Yu, H. Fabrication of Gradient-Structure CuNiBe Alloy Bars by Laser Remelting and Water-Cooling. *Mater. Manuf. Process.* 2020, 35(3), 337–345. DOI: 10.1080/10426914.2020.1726948.
- Teng, Y. L.; Li, L.; Zhang, W.; Wang, N.; Feng, C. C.; Ren, J. H. Machining Characteristics of PCD by EDM with Cu-Ni Composite Electrode. *Mater. Manuf. Process.* 2020, 35(4), 442–448. DOI: 10.1080/10426914.2020.1718700.
- Shahid, M. B.; Han, S. C.; Jun, T. S.; Park, D. S. Effect of Process Parameters on the Joint Strength in Ultrasonic Welding of Cu and Ni Foils. *Mater. Manuf. Process.* 2019, 34(11), 1217–1224. DOI: 10.1080/10426914.2019.1643474.
- Reisgen, U.; Olschok, S.; Jakobs, S.; Turner, C. Sound Welding of Copper: Laser Beam Welding in Vacuum. *Phys. Procedia*. 2016, 83, 447–454. DOI: 10.1016/j.phpro.2016.08.046.
- Darji, R.; Badheka, V.; Mehta, K.; Joshi, J.; Yadav, A. Processing of Copper by Keyhole Gas Tungsten Arc Welding for Uniformity of Weld Bead Geometry. *Mater. Manuf. Process.* 2020, 1–10. DOI: 10.1080/10426914.2020.1784932.
- Wang, L.; Li, X.; Gao, M.; Stabilization Mechanism, Z. X. Weld Morphological Features of Fiber Laser-Arc Hybrid Welding of Pure Copper. *J. Manuf. Process.* 2017, 27, 207–213. DOI: 10.1016/j.jmapro.2017.05.009.
- Brooks, R. F.; Egly, I.; Seetharaman, S.; Grant, D. Reliable Data for High-Temperature Viscosity and Surface Tension: Results from a European Project. *High Temp. - High Press.* 2001, 33(6), 631–637. doi:10.1068/htwu323.
- Hess, A.; Schuster, R.; Heider, A.; Weber, R.; Graf, T. Continuous Wave Laser Welding of Copper with Combined Beams at Wavelengths of 1030 Nm and of 515 Nm. *Phys. Procedia*. 2011, 12(PART 1), 88–94. DOI: 10.1016/j.phpro.2011.03.012.
- Zhang, L. J.; Ning, J.; Zhang, X. J.; Zhang, G. F.; Zhang, J. X. Single Pass Hybrid Laser-MIG Welding of 4-Mm Thick Copper without Preheating. *Mater. Des.* 2015, 74, 1–18. DOI: 10.1016/j.matdes.2015.02.027.
- Lin, J. W.; Chang, H. C.; Wu, M. H. Comparison of Mechanical Properties of Pure Copper Welded Using Friction Stir Welding and Tungsten Inert Gas Welding. *J. Manuf. Process.* 2014, 16(2), 296–304. DOI: 10.1016/j.jmapro.2013.09.006.
- Yinan, L.; Shanbin, Z.; Zilong, P.; Feng, G. A Study on the Mechanism of Crystal Cracking in GTA Welding of Copper Plates. *Mater. Manuf. Process.* 2016, 31(16), 2143–2151. DOI: 10.1080/10426914.2015.1103861.
- Miyagi, M.; Zhang, X. Investigation of Laser Welding Phenomena of Pure Copper by X-Ray Observation System. *J. Laser Appl.* 2015, 27(4), 042005. DOI: 10.2351/1.4927609.
- Dak, G.; Joshi, J.; Yadav, A.; Chakraborty, A.; Khanna, N. Autogenous Welding of Copper Pipe Using Orbital TIG Welding Technique for Application as High Vacuum Boundary Parts of Nuclear Fusion Devices International Journal of Pressure Vessels

- and Piping Autogenous Welding of Copper Pipe Using Orbital TIG Welding. *Int. J. Press. Vessel. Pip.* **2020**, *188*(December), 104225. doi:10.1016/j.ijvpv.2020.104225.
- [24] Weldability of Materials - Copper and Copper Alloys - TWI <https://www.twi-global.com/technical-knowledge/job-knowledge/weldability-of-materials-copper-and-copper-alloys-023> (accessed Sep 17, 2020).
- [25] Chikova, O. A.; Tkachuk, G. A.; V'yukhin, V. V. Viscosity of Cu-Ni Melts. *Russ. J. Phys. Chem. A.* **2019**, *93*(2), 198–203. DOI: 10.1134/S0036024419020067.
- [26] Darji, R. S.; Joshi, G. R.; Oza, A. D.; Badheka, V. J. Exploiting the Challenges of Copper to Austenitic Stainless Steel Bimetallic Joining by Gas Tungsten Arc Welding: A Fluid Flow Perspective. *IOP Conf. Ser. Mater. Sci. Eng.* **2021**, *1146*(1), 012011. DOI: 10.1088/1757-899x/1146/1/012011.
- [27] Camurri, C.; Lopez, M.; Fernandez, R.; Osorio, V. Copper Welding with Copper Filler. *Weld. Int.* **1996**, *10*(5), 387–389. DOI: 10.1080/09507119609549014.
- [28] Hao, K.; Gong, M.; Xie, Y.; Gao, M.; Zeng, X. Effects of Alloying Element on Weld Characterization of Laser-Arc Hybrid Welding of Pure Copper. *Opt. Laser Technol.* **2018**, *102*, 124–129. DOI: 10.1016/j.optlastec.2017.12.029.
- [29] Davis, J. R. *Copper and Copper Alloys*, ASM Speciality Handbook, ASM International, **2001**; pp 32–33.
- [30] Dieter, G. E. *Mechanical Metallurgy*; McGraw-Hill Book Company, **2009**; pp 203–207.
- [31] Zhang, J.; Shen, Q.; Luo, G.; Li, M.; Microstructure, Z. L. Bonding Strength of Diffusion Welding of Mo/Cu Joints with Ni Interlayer. *Mater. Des.* **2012**, *39*, 81–86. DOI: 10.1016/j.matdes.2012.02.032.
- [32] Zhang, L. J.; Bai, Q. L.; Ning, J.; Wang, A.; Yang, J. N.; Yin, X. Q.; Zhang, J. X.; Comparative, A. Study on the Microstructure and Properties of Copper Joint between MIG Welding and Laser-MIG Hybrid Welding. *Mater. Des.* **2016**, *110*, 35–50. DOI: 10.1016/j.matdes.2016.07.117.
- [33] Chiocca, A.; Soulié, F.; Bordreuil, C.; Bordreuil, C. In Situ Observations and Measurements during Solidification of CuNi Weld Pools in Situ Observations and Measurements during Solidification of CuNi Weld Pools. *Sci. Tech. Weld. Join.* **2016**, *1718*(July). doi: 10.1179/1362171815Y.0000000091.
- [34] 70/30 Cupronickel, Columbia Metals. Enhanced Reader. <https://www.columbiametals.com/files/products/96.pdf> (accessed Dec 11, 2020).